J Mater Sci (2010) 45:6769–6774
DOI 10.1007/s10853-010-4773-0

Synthesis and characterization of mesoporous silicon directly from pure silica sodalite single crystal

Jiang Zhu · Jian Wu · Yu Wang · Changgong Meng

Received: 1 February 2010 / Accepted: 15 July 2010 / Published online: 27 July 2010

Abstract Mesoporous silicon granules with high surface area were synthesized directly from pure silica sodalite single crystals, with the starting shape retained. The sodalite single crystals were reduced by a magnesiothermal process in vacuum at 630 °C. The X-ray diffraction patterns indicate the presence of crystal silicon. Transmission electron microscopy studies reveal that the obtained silicon granules are composed of a monocrystalline surface with an island-like mesoporous internal structure. The results of N_2 adsorption and desorption analysis indicate that the surface area is around 308 m^2 g^{-1} and the single point pore volume is 0.37 cm^3 g^{-1}. The photoluminescence emission centered at 2.7 eV may be due to both an oxidized surface and quantum confinement effects. These results reveal that the silicon granules possess a different microstructure from those of etched silicon films. The present synthetic design correlates the microporous zeolite and mesoporous silicon together and gives a new way for enlarging the structural diversity of porous silicon crystal.

Abbreviations

SOD	Sodalite
XRD	X-ray powder diffraction
SEM	Scanning electron microscope
TEM	Transmission electron microscope
HRTEM	High-resolution TEM
SAED	Selected area electron diffraction
EDS	Energy dispersion spectrometer
PL	Photoluminescence
BET	Brunauer–Emmet–Teller
LO	Longitudinal optical phonon
TA	Transverse acoustical phonon
TO	Transverse optical phonon

Electronic supplementary material The online version of this article (doi:10.1007/s10853-010-4773-0) contains supplementary material, which is available to authorized users.

J. Zhu · J. Wu · Y. Wang · C. Meng (✉)
Chemistry Department, Dalian University of Technology, Dalian 116023, China
e-mail: cgmeng@dlut.edu.cn

Introduction

Since Canham discovered the strong visible luminescence from porous silicon at room temperature in 1990 [1], this material has been found of many applications in sensors, biomedicine, MEMS, and energy, resulting from its unique structure and optical properties [2–6]. The first reported observation of porous silicon is from Uhlir who was developing an electrochemical polishing method for crystalline silicon and germanium [7]. From then on porous silicon was traditionally synthesized from silicon wafer via chemical or electrochemical etching methods. The doping of the substrate plays a critical role in determining the nature of porous silicon and the pore properties can be adjusted by temperature, potential, etching time, the components concentrations in etching solution, and so on [8, 9]. The deep pores always grow along the <100> direction and usually perpendicular to the wafer surface, connecting to each other to form three-dimensional structures upon further etching [10]. However, the similar etching process resulted in similar structures, which limits the variety of porous silicon structures, thus the study of synthesis and characterization of porous silicon materials with new structures is one of the most important subjects in the research of material field. In recent years, displacement reaction began to be used in porous silicon preparation.

Displacement reaction has been used to synthesize bulk silicon, with different form of silicon oxides or silicides reduced directly by metals [11, 12]. It was first reported that porous silicon was prepared by a displacement reaction in 2003 [13]. Through a pinpoint and bulk electrochemical process, porous silicon was prepared from quartz plate in molten calcium chloride electrolyte at 850 °C when a molybdenum or tungsten wire was used as electrode [14]. Bao and Sandhage successfully converted nanostructured microshells of diatoms into microporous silicon replicas at 650 °C through a spontaneous process, with the 100 nm pores remaining [15]. More recently, it has been reported that Mediterranean sand was reduced to porous silicon under the auto pressure at 750 °C [16]. However, previous research has neglected a special group form of silica, the pure silica zeolites. Pure silica zeolites are a particularly interesting group with high thermal stability and diverse ordered channels and pores in their structures [17–21]. In this article, we first correlate these two porous materials together directly. Pure silica sodalite (SOD type) single crystals were converted into mesoporous silicon granule with high surface area by a magnesiothermal reduction process in vacuum, during which the original shape and fine features were well preserved. Our reaction design uses a modest temperature (630 °C) and the reactant is an easily obtained material with abundant structures, which permits the development of different structures under relatively modest conditions.

Experimental

Material synthesis

SOD type single crystals were synthesized by a typical hydrothermal method using pyrocatechol as the template and glycol as the solvent. The composition of the gel is as following: molar ratio SiO_2:NaOH:pyrocatechol:glycol = 6.5:2.5:1:50. After reaction at 170 °C for 7 days, the product was filtered and washed with water and ethanol several times. The as-synthesized single crystals were dried at 100 °C for 2 h and then calcined at 550 °C for 5 h in air.

A typical method for the reduction reaction is as following: a mixture of magnesium powder and SOD type single crystals (0.6 g, molar ratio $Mg:SiO_2 = 2.5:1$) was placed in a ceramic boat in a tube furnace. After the furnace was evacuated, the mixture was heated to a temperature ranging from 630 to 650 °C and maintained for 2 h. The products were collected and immersed in HCl solution (with molar ratio of $HCl:H_2O:EtOH = 0.50:3.57:6.73$) for 6 h at room temperature to selectively remove the magnesia and excessive Mg powder and leave only trace silica and structured silicon. The sample was then exposed to a HF solution (with molar ratio of $HF:H_2O:EtOH = 0.70:0.74:5.92$) for 10 min to ensure that any oxide unreacted or formed during the HCl treatment was eliminated completely. Finally, the obtained silicon granules were dried at 100 °C for 4 h. The average yield is about 90%. When the molar ratio of $Mg:SiO_2$ is less than 2:1, the average yield decreases to no more than 80%; when the molar ratio of $Mg:SiO_2$ increases to more than 3:1, Mg_2Si begins to be found in the products. If the reaction temperature is lower than 620 °C, the reaction does not take place; if the temperature is higher than 700 °C, some granules begin to crack on the surface.

Characterization

The X-ray powder diffraction (XRD) analysis was taken to verify the sample structure using a Shimadzu XRD-6000 diffractometer with Cu Kα radiation ($\lambda = 1.54060$ Å), operating at a voltage of 40 kV and a current of 30 mA. The morphologies were observed by a JSM-5600LV scanning electron microscope (SEM) operated at 5.0 kV. Transmission electron microscope (TEM) and high-resolution TEM (HRTEM) images were obtained with a Philips Tecnai G^2 20 instrument, which was equipped with selected area electron diffraction (SAED) and operated with an accelerating voltage of 200 kV. The silicon granules were broken into pieces by ultrasonication to ensure that the pieces of granules were thin enough for the TEM measurement. The Raman spectrum was obtained at room temperature on a Raman DPG1-2200, using an Ar^+ laser as excitation with a wavelength of 532 nm and 10 mW power. The photoluminescence (PL) emission spectrum was measured with a Fluorescence Spectrometer (Perkin Elmer LS55) using a xenon lamp as the excitation source. The N_2 adsorption–desorption isotherm was obtained by using a Micrometrics ASAP-2020 analyzer.

Results and discussion

To confirm the success of the reaction, we used the XRD to examine the components of the products before and after the wash with HCl and HF. Figure 1a shows the XRD pattern of reacted specimens after reduction reaction, which reveals the presence of crystal silicon (pdf 27-1402) and MgO (pdf 77-2179), as well as excess magnesium (pdf 35-0821). After the wash with HCl and HF solutions, only sharp peaks attributed to crystal silicon were observed in the XRD pattern shown in Fig. 1b, indicating that the residual impurities were efficiently removed. Thus, the reduction of SiO_2 to Si had been confirmed.

Figure 2a shows a representative SEM image of SOD type single crystals. Each uniform granule possesses a

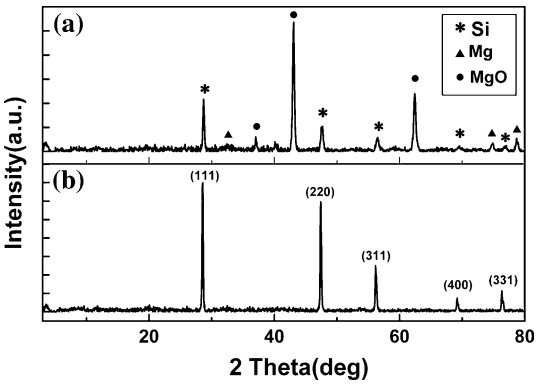

Fig. 1 XRD patterns with the samples after reduction (**a**) and after treatments of HCl and HF solutions (**b**)

perfect cubic shape and fine features, with the edge about 20 μm long. As revealed in Fig. 2b, the cubic shape was well retained after the reduction and the subsequent wash with HCl and HF, with no measurable change in the size of the granule. The modest temperature and appropriate reaction time prevent the shape from distorting and collapsing. Meanwhile, the formation of a magnesia phase penetrating into the crystal silicon granule also solidifies the framework of the granule. As a result, the original cubic shape is well preserved. As shown in Fig. 2c, if the reaction temperature was increased above 700 °C, or the reaction time was prolonged to more than 4 h, the surface of some granules cracked. Figure 2d clearly reveals that a part surface of a granule was desquamated during the reaction. The porous structure under the surface is clearly observed, with numbers of grains conglomerating together.

TEM analysis was conducted on the cross sections of as-synthesized silicon granules to confirm the microstructures. The images clearly demonstrated that the sample is composed of two structures: lamellar piece and island-like porous morphology. The low magnification TEM image shown in Fig. 3a represents a relatively large lamellar piece with smooth surface. The uniform and homogeneous contrast on the piece reflects its uniform thickness. The HRTEM image, shown in Fig. 3b, suggests a monocrystalline structure with a uniform lattice spacing of approximately 0.32 nm, which is consistent with the spacing between the (111) planes in a face-centered cubic crystal silicon. The SAED pattern in the inset has sharply diffracted spots assigned to the [110] plane, also confirming the monocrystal morphology in this area. The TEM image of the island-like mesoporous structure is presented in Fig. 3c. Particles join together to form a three-dimensional

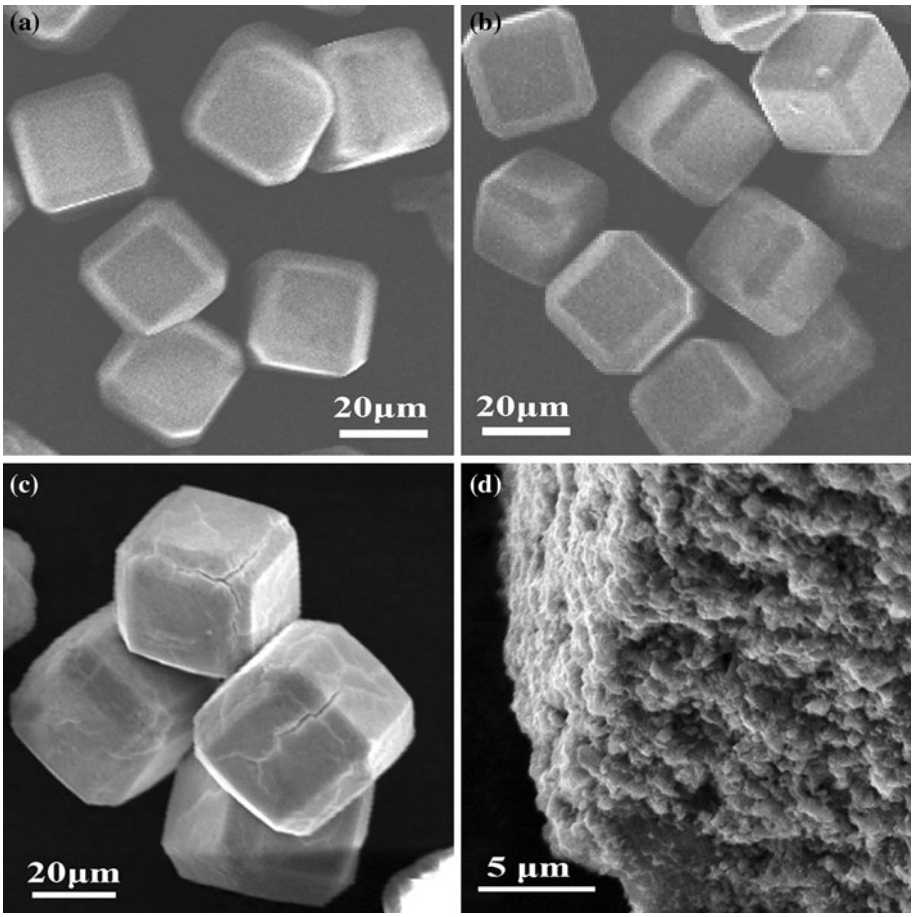

Fig. 2 SEM images of SOD type pure silica zeolite single crystals (**a**), the as-synthesized silicon granules after treatments with HCl and HF solutions (**b**), some granules cracked on the surface (**c**), and part of the porous structure under the surface (**d**)

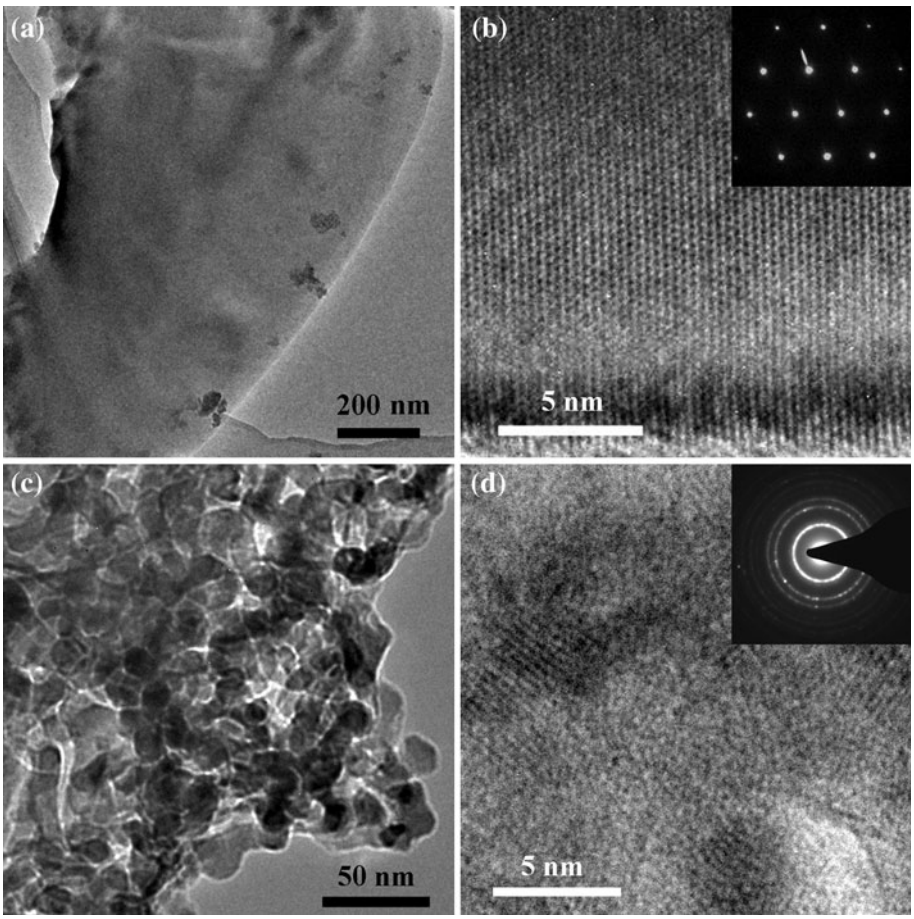

Fig. 3 TEM image (**a**) and HRTEM image (**b**) of a lamellar monocrystal piece from a silicon granule, in the *inset* of (**b**) is the corresponding SAED pattern. TEM image (**c**) and HRTEM image (**d**) of the island-like mesoporous structure from a silicon granule, in the *inset* of (**d**) is the corresponding SAED pattern

island-like structure. Most of the particles have a relatively uniform diameter of about 15–20 nm. Some were observed to be dark in the image, mainly due to the overlapping of adjacent portions. The disordered spaces between the islands may come from the rearrangement of bonds of ordered SOD cages, owing to the added porosity caused by the loss of oxygen. Figure 3d shows a HRTEM image of the islands structure. There are many crystalline silicon nanodots approximately 5 nm in diameter, as indicated by the lattice fringes with different orientations. The interplanar spacing of the crystal state is about 0.32 nm, matching very well with the (111) planes of crystal silicon. The inset is the SAED pattern in which well-defined diffraction rings also match with polycrystalline silicon [22].

Energy dispersive spectrometry (EDS) was used to determine the real composition of the sample. The EDS data, Fig. 4, show strong signals for C, O, Cu, and Si. The occurrence of the Cu peak is due to the Cu grid used for the TEM sample, while the C peak originates from the C film coating on the Cu grid. The low concentration of O may come from a small amount of oxidized sample. Compared with the intensity of Si peaks, the intensity of O peaks is very low, as shown in the full-scaled EDS analysis in the inset of Fig. 4. As the EDS microanalysis of oxygen is not

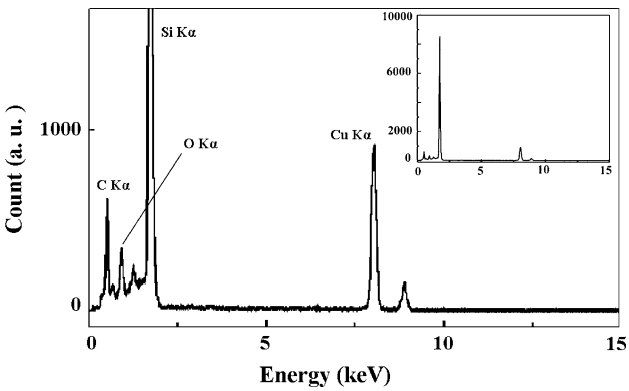

Fig. 4 EDS results of an area of the island-like mesoporous structure from a silicon granule observed in TEM analysis and the full-scaled EDS results are shown in the *inset*

accurate, we could only conclude that there exists a small amount of oxygen in the Si granules, due to exposure to air during drying and introduction into the chamber [23].

The N_2 adsorption–desorption isotherm of the sample obtained at −196 °C, Fig. 5, shows a representative type IIb curve with abrupt change in the relative pressure range of 0.8–0.9, where the mesoporosity only arises from interparticle interactions [24]. The type H4 hysteresis loop

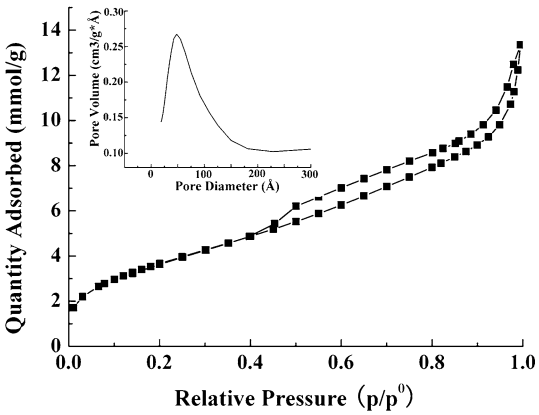

Fig. 5 Nitrogen adsorption–desorption isotherms of the synthesized porous silicon granules and pore size distribution are shown in the *inset*

appears at p/p^0 of 0.5–1.0 and the two branches are nearly parallel and horizontal over a wide range, indicating the presence of narrow slit-like pores [25]. The Brunauer–Emmet–Teller (BET) report showed that the sample has a high surface area of 308 $m^2\ g^{-1}$ and the single point pore volume is 0.37 $cm^3\ g^{-1}$ at a relative pressure (p/p^0) of 0.973. A single peak in the BET pore distribution at 48 Å is observed in the inset of Fig. 5, indicating a relatively uniform mesopores.

Raman spectroscopy is a helpful tool to obtain information about structure, bonding, and disorder in porous silicon, since the wavenumbers and relative intensities of vibrations and phonons are dependent on the structure and chemical environment, and depolarization factors are dependent on the structure and level of disorder [16]. The Raman spectrum of the sample is shown in Fig. 6a. The 520 cm^{-1} line can be assigned to bulk crystal silicon, matching the observation in TEM [26]. Normally the intensity of 636 cm^{-1} line of longitudinal optical phonon (LO) and transverse acoustical phonon (TA) modes in crystal silicon is close to zero at room temperature. Here, the 634 cm^{-1} line is due to the combination of the second-order spectrum of LO and TA modes, which is enhanced by the relaxation of selection rules and surface assistance [27]. The broadening of the 970 cm^{-1} line is ascribed to the second-order Raman scattering of transverse optical phonon (TO) mode at surface of crystal silicon or porous silicon [27, 28]. Thus, we can propose that the monocrystal silicon may come from the surface of the granule, with a more porous structure enclosed by this monocrystal structure. The possible shifted bands arising from porous silicon may be hidden by the intense lines from crystalline silicon, due to the accuracy of the instrument.

One of the most important properties of porous silicon is its PL. The PL spectrum at room temperature, Fig. 6b, shows an emission in the blue region centered at about 460 nm (2.7 eV), with an excitation at 286 nm. This blue emission has been ascribed to quantum confinement effect, oxide defects, or surface state [26, 29]. In our experiment, the sample was treated by HCl and HF solutions, during or after which parts of the surface may be oxidized. The existence of Si–O bonds was confirmed by the FTIR spectrum for the sample (Fig. S1 in Supplementary Information). The FTIR also shows no detectable Si–H band, suggesting that the surface oxidation is complete. The diameter of polycrystal silicon grains observed in TEM analysis is about 5 nm, falling into the quantized range, which may also contribute to the blue emission. Therefore, we attribute this blue emission to the combined result of an oxidized surface and quantum confinement effect. The typical peak of porous silicon at 680 nm is not seen, which suggests that the luminescence from the silicon nanocrystallites is weak relative to the observed PL signal.

The exploration and understanding of the reaction mechanism for the formation of porous silicon from sodalite crystals is not easily accessible. According to the results of SEM, TEM, and Raman spectrum, it is reasonable to assume that the monocrystal pieces come from the surface of the granule and the mesoporous structure comes from the inside. During the reaction, Mg rapidly reacts with the surface of the granule. The homogeneous surface is directly reduced to the monocrystal structure. In view of the differences between the surface and the inside, hollow

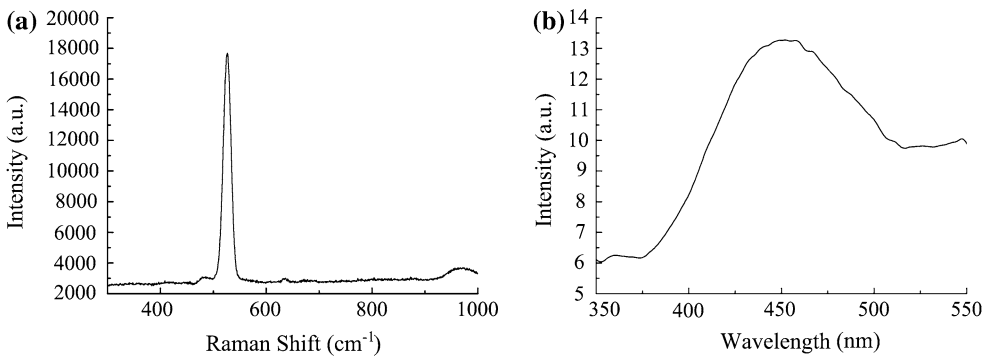

Fig. 6 Raman spectrum (**a**) and photoluminescence spectrum (**b**) of the of the synthesized porous silicon granules

locations occur on the interface [30]. When Mg continues to enter the inside and the SOD cages begins to be broken, the formation of MgO increases the porosity volume and leads to the crack formation. The island-like porous structure could be interpreted by a combination result of the original porous structure and the elimination of the MgO. The distortion to the lattice appears to be primarily a result of thermal contraction and defects of Si–Si bond from Si–O–Si bond, where the oxygen atom is seized by Mg. There is no system collapse or phase change in this process. Solid-phase crystallization from SiO_2 to silicon takes place via the bond rearrangement process.

However, we have to admit that this is the only speculation and the further related study is currently under way.

Conclusions

In conclusion, we have demonstrated that mesoporous silicon granules with high surface area have been synthesized from SOD type single crystals. Two kinds of structures including island-like mesoporous structure and monocrystal piece have been found in the retained cubic shape. A reasonable mechanism has been proposed on the basis of convincing experimental evidence. We believe that the particular structure and properties of the silicon granules may have potential applications in optical devices, separation media, or sensors. This general approach is applicable to the further extensive study of the new structures of porous silicon.

Acknowledgements The authors are grateful to Experimental Center of Chemistry, Dalian University of Technology (China) for providing the necessities in experiments. Many thanks are dedicated to Mr. Shouhua Ji and Mr. Longjiang Zou for their continuous support.

References

1. Canham LT (1990) Appl Phys Lett 57(10):1046
2. Mizsei J (2007) Thin Solid Films 515:8310
3. Zhao Y, Li D, Sang W, Yang D, Jiang M (2007) J Mater Sci 42:8496. doi:10.1007/s10853-007-1749-9
4. Torres-Costa V, Martin-Palma RJ (2010) J Mater Sci 45:2823. doi:10.1007/s10853-010-4251-8
5. Pichonat T, Gauthier-Manuel B (2007) Microsyst Tech 13:1671
6. Plessis M (2007) Sens Actuators A Phys 135(2):666
7. Uhlir A (1956) Bell System Tech J 35:333
8. Ohmukai M, Okada K, Tsutsumi Y (2005) J Mater Sci: Mater Electron 16:119
9. Zhao Y, Li D, Yang D (2006) J Mater Sci 41:5283. doi:10.1007/s10853-006-0267-5
10. Chuang SF, Collins SD, Smith RL (1989) Appl Phys Lett 55(7):675
11. Breslin MC, Ringnalda J, Xu L, Fuller M, Seeger J, Daehn GS, Otani T, Fraser HL (1995) Mater Sci Eng A 195:113
12. Biehl E, Schubert U, Kubel F (2001) New J Chem 25:994
13. Nohira T, Yasuda K, Ito Y (2003) Nat Mater 2:397
14. Jin X, Gao P, Wang D, Hu X, Chen G (2004) Angew Chem Int Ed 43:733
15. Bao Z, Weatherspoon MR, Shian S, Cai Y, Graham PD, Allan SM, Ahmad G, Dickerson MB, Church BC, Kang Z, Abernathy HW III, Summers CJ, Liu M, Sandhage KH (2007) Nature 446:172
16. Hai NH, Grigoriants I, Gedanken A (2009) J Phys Chem C 113:10521
17. Shanbhag GV, Choi M, Kim J, Ryoo R (2009) J Catal 264:88
18. Gu LJ, Ma D, Yao SD, Liu X, Han X, Shen W, Bao X (2009) Chem Eur J 15:13449
19. Cooper CA, Lin YS (2007) J Mater Sci 42:320. doi:10.1007/s10853-006-1020-9
20. Li Z, Marler B, Gies H (2008) Chem Mater 20:1896
21. Trzpit M, Soulard M, Patarin J (2009) J Mater Sci 44:6525. doi:10.1007/s10853-009-3579-4
22. Liu S, Kobayashi M, Sato S, Kimura K (2005) Chem Commun 37:4690
23. Richman EK, Kang CB, Brezesinski T, Tolbert SH (2008) Nano Lett 8:3075
24. Huo Q, Zhao D, Feng J, Weston K, Buratto SK, Stucky GD, Schacht S, Schüth F (1997) Adv Mater 9:974
25. Hilonga A, Kim J, Sarawade PB (2010) J Mater Sci 45:1264. doi:10.1007/s10853-009-4077-4
26. Yang S, Cai W, Zeng H, Li Z (2008) J Appl Phys 104:023516-1
27. Salcedo WJ, Fernandez FJR, Rubim JC (1999) J Raman Spectrosc 30:29
28. Tanino H, Kuprin A, Deai H (1996) Phys Rev B 53:1937
29. Li XX, Tang YH, Lin LW, Li JL (2008) Microporous Mesoporous Mater 111:591
30. Martin-Palma RJ, Pasual L, Herrero P, Martinez-Duart JM (2002) Appl Phys Lett 81:25